Biophysics

Deutsche Ausgabe: DOI: 10.1002/ange.201504247
Internationale Ausgabe: DOI: 10.1002/anie.201504247

Condensation Agents Determine the Temperature–Pressure Stability of F-Actin Bundles

*Mimi Gao, Melanie Berghaus, Julian von der Ecken, Stefan Raunser, and Roland Winter**

Abstract: *Biological cells provide a large variety of rodlike filaments, including filamentous actin (F-actin), which can form meshworks and bundles. One key question remaining in the characterization of such network structures revolves around the temperature and pressure stabilities of these architectures as a way to understand why cells actively use proteins for forming them. The packing properties of F-actin in fascin- and Mg^{2+}-induced bundles are compared, and significantly different pressure-temperature stabilities are observed because of marked differences in their nature of interaction, solvation, and packing efficiency. Moreover, differences are observed in their morphologies and disintegration scenarios. The pressure-induced dissociation of the actin bundles is reminiscent of a single unbinding transition as observed in other soft elastic manifolds.*

Condensation of highly charged biopolymers such as DNA, microtubules, and filamentous actin (F-actin) is fundamental for maintaining cellular architecture. This condensation allows efficient packing of the genetic information and provides cell shape, integrity, and movement. In vivo, the like-charge attraction between such polyelectrolytes is realized with the aid of specific binding proteins,[1] whereas it can be observed in the presence of multivalent counterions and polymers in vitro.[2] The lateral condensation and thus bundling of F-actin plays a key role in the formation of filopodia, invadopodia, microvilli, stress fibers, and hair cells.[3] The geometries and mechanical properties of these bundles (B-actin) highly depend on the shape and size of the cross-linking protein.[4] In contrast, high concentrations of divalent ions (intracellular $[Mg^{2+}]$ can be up to 10 mM) have been found to induce like-charge attractions between polyelectrolytes in vitro and thus bundle F-actin. Small-angle X-ray scattering (SAXS) studies revealed that the divalent ions condense into ripple-like charge layers coating the actin filaments.[2,5] However, bundling of F-actin occurs naturally in the cytoplasm of cells, which is typically filled up to a volume of 30–40% by different macromolecules.[6] Independent studies revealed that depletion forces induced by highly concentrated poly(ethylene glycol) solutions feature bundling activity without incorporating the polymer into the actin bundles.[7] This observation raises the question as to why cells actively use proteins rather than depletion forces and divalent ions for F-actin bundling when they are ubiquitously present in the cytoplasm. The sum of all interactions (electrostatics, dispersion forces, depletion interaction, hydration repulsion, and entropic repulsion), which generally determines the structure and dynamics of such biopolymer networks, leads one to expect a rich and complicated phase behavior and intricate microstructures. To shed light on this question, we use here the complementary tools SAXS and transmission electron microscopy (TEM) to compare the bundle morphology, the packing geometry of F-actin in bundles formed by fascin[8] (the key bundling protein in filopodia) and Mg^{2+}, as well as their stability as a function of temperature and pressure.

SAXS intensity profiles at $T = 20\,°C$ ($p = 0.1$ MPa) indicate a hexagonal packing of the filaments for both types of bundles (Figure 1). For the fascin-induced bundles, these are the first-order peaks at the position $q_{10} = 0.585\ nm^{-1}$ and $q_{20} = 2q_{10}$. The corresponding hexagonal lattice constant $d = 4\pi/\sqrt{3}q_{10}$ amounts to 12.4 nm (Figure 1 A).[9] The ratio of the peak positions (1:2) indicates a perfect hexagonal packing of the fascin-connected filaments. The peak intensity decreases drastically between 52.5 and 55 °C, thus indicating a melting/degradation temperature (T_M) of the bundles of

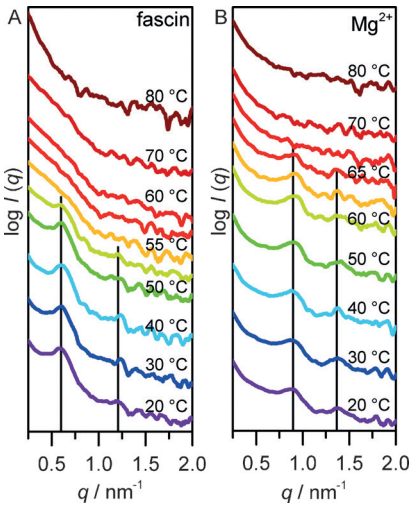

Figure 1. Temperature-dependent SAXS intensity profiles of B-actin. Bundling of F-actin was induced with either fascin (A) or Mg^{2+} ions (B). Black solid lines indicate the position of the peak maxima related to hexagonal packing of filaments at 20 °C (A and B). Curves were shifted for clarity.

[*] M. Gao,[+] M. Berghaus,[+] Prof. Dr. R. Winter
Physical Chemistry I—Biophysical Chemistry
Faculty of Chemistry and Chemical Biology, TU Dortmund
Otto-Hahn-Strasse 6, 44227 Dortmund (Germany)
E-mail: roland.winter@tu-dortmund.de
J. von der Ecken, Prof. Dr. S. Raunser
Department of Structural Biochemistry, Max Planck Institute of Molecular Physiology, 44227 Dortmund (Germany)
[+] These authors contributed equally to this work.

Supporting information for this article is available on the WWW under http://dx.doi.org/10.1002/anie.201504247.

about 54 °C. With increasing temperature, the peak position and thus the lattice constant (d) does not change markedly. A small (0.3 nm) decrease is observed from 20 to 40 °C, only, and the d value starts to increase again above 50 °C when dissociation of the bundles sets in (see Figure S1 in the Supporting Information). From 55 to 70 °C, the SAXS intensity profiles resemble the scattering pattern of F-actin,[9] and is in agreement with the scattering pattern of randomly orientated F-actin as displayed in Figure S2. Both SAXS profiles show a slight increase of the intensity in the q-range where broad diffraction peaks (at 1.14 and 1.25 nm^{-1}) associated with the helical structure of F-actin were found in ordered F-actin bundles.[9] However, our data indicate that the thermal degradation of bundles proceeds by the dissociation of the filaments. From 70 to 80 °C, a further change of the SAXS profile can be observed (see Figure 1 A and Figure S2A), and is similar to the change in the scattering curve of F-actin upon thermal denaturation with a T_M of 75 °C.[10] These changes include a drastic increase of the scattering intensity at low q values, which is indicative of protein aggregation. The according pair-distance distribution function, $p(r)$, suggests a transition from a cylindrical, elongated species to slightly elongated aggregates with a radius of gyration of about 10 nm (see Figure S2B).

The SAXS profile of the Mg^{2+}-induced bundles at 20 °C reveals a first-order peak at $q_{10} = 0.85\ nm^{-1}$ and a weak higher-order peak at 1.36 nm^{-1} (Figure 1 B). The ratio of the two peaks (1:1.6) differs slightly from the $1:\sqrt{3}$ ratio expected for a perfect hexagonal packing. The first-order peak is associated with a hexagonal lattice constant of 8.5 nm, which reflects closest packing of actin filaments.[5] No significant shift of the diffraction peaks and hence d values is observed with increasing temperature up to 40 °C. However, the d value decreases from about 8.5 to 8.1 nm between 40 and 62.5 °C (see Figure S1). The peak intensity drastically decreases between 65 and 67.5 °C, thus indicating a melting temperature of the Mg^{2+}-induced actin bundles of about 66 °C, which is in good agreement with FTIR spectroscopic measurements.[10] In contrast to the fascin-induced bundles, a scattering profile reflecting the characteristics of F-actin cannot be observed at any temperature. Instead, the scattering profiles of the Mg^{2+}-induced bundles above 65 °C suggests direct formation of amorphous actin aggregates from the bundles after dissociation.

Complementary TEM images reveal significant differences between the morphology of the bundles formed by fascin and Mg^{2+} ions, respectively, thus indicating different underlying molecular interaction mechanisms (Figure 2 A and B). At ambient conditions, fascin induces the formation of rigid and planar bundles with a homogenously distributed thickness. In contrast, more flexible, tubular, and differently sized bundles are formed in the presence of Mg^{2+}. By exhaustive screening of several prepared specimens at low magnification, significantly shorter bundles are observable in the presence of fascin compared to those with Mg^{2+}. However, in both cases the bundles feature periodic transverse banding patterns, thus indicating orderly and hexagonal packing. At a molar ratio of 1:4 of fascin and globular actin monomer (G-actin), all actin filaments are bundled, whereas

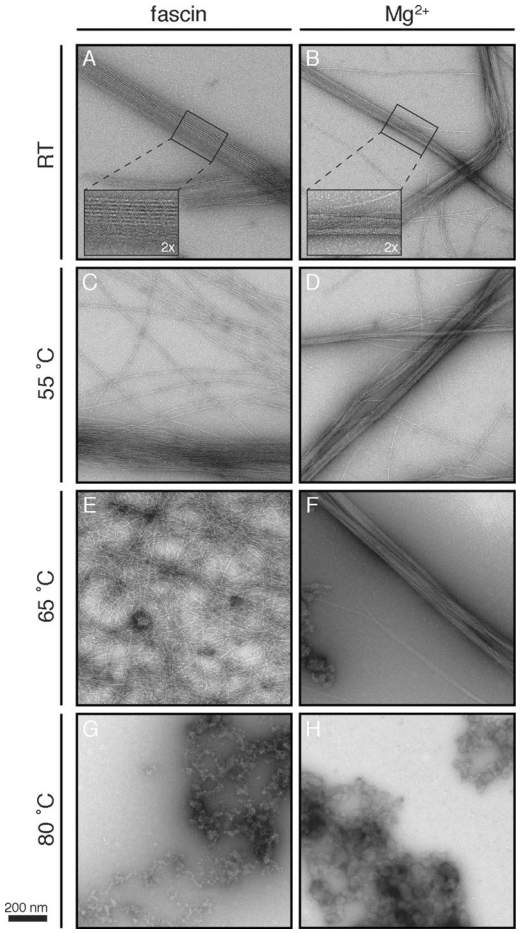

Figure 2. Thermal stability of F-actin bundles condensed by fascin and Mg^{2+}. Representative transmission electron micrographs show the morphology of B-actin at room temperature (A and B) and after heating up to 55 (C and D), 65 (E and F), and 80 °C (G and H) for 10 min.

in the presence of 50 mM Mg^{2+} ions, isolated F-actin molecules are still detectable. Increasing the temperature up to 55 °C causes dissociation of the fascin-induced bundles into F-actin, whereas the morphology of the Mg^{2+}-induced species is not significantly affected (Figure 2 C and D). Further, the dissociation leads to formation of free actin filaments which are longer than those within the bundles, thus indicating immediate assembly of short actin filaments along their long axis. This behavior reflects the intactness of F-actin upon dissociation from the bundles. At 65 °C, no bundles are present, but shrunk filaments and first amorphous aggregates are formed for the fascin-induced species (Figure 2 E). In contrast, during thermal denaturation Mg^{2+}-induced bundles directly aggregate into amorphous protein clusters rather than dissociate into F-actin, which is consistent with our SAXS data (Figure 2 F). These observations imply that the interfilament interactions of electrostatic nature are stronger than the intrafilament interactions. Finally, when heating up to 80 °C, both bundle types aggregate completely (Figure 2 G and H).

Studying the response of fascin- and Mg^{2+}-induced actin bundles to high hydrostatic pressure with SAXS reveals that

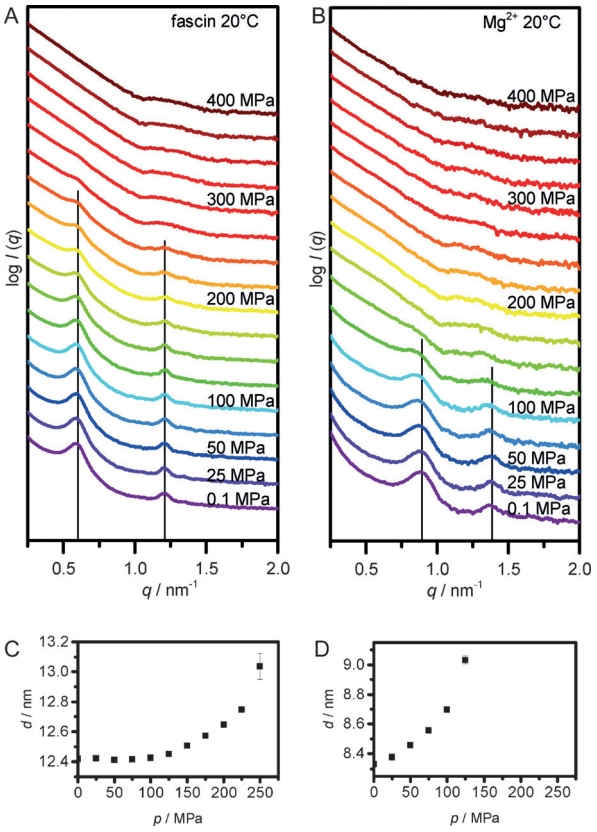

Figure 3. Pressure-dependent synchrotron small-angle X-ray scattering data of B-actin at 20 °C. Bundling of the F-actin was induced with either fascin (A and C) or Mg^{2+} ions (B and D). A,B) Intensity profiles are shown with black solid lines indicating the position of the peak maxima related to a hexagonal packing of the filaments at 0.1 MPa. Curves were shifted for clarity. C,D) Pressure-dependent changes of the lattice constant.

these actin bundles are present up to a pressure of about 250 and 160 MPa, respectively (Figure 3). For fascin-induced bundles, the peak position does not change significantly from 0.1 up to a pressure of 125 MPa, while between 125 and 250 MPa a marked shift towards lower q values is observed (Figure 3 A). The calculated lattice constant, $d(p)$, shows a total increase of the intermolecular distance between the filaments of about 0.6 nm between 125 and 250 MPa (Figure 3 C). After dissociation, from about 250 up to the maximum pressure of 400 MPa, the observed intensity profile monitored is characteristic for F-actin. In contrast, the scattering intensity profiles of the Mg^{2+}-induced actin bundles (Figure 3 B) and the pressure-dependent changes of the lattice constant (Figure 3 D) show a continuous shift of the q_{10}-peak towards lower q values up to the dissociation pressure. The lattice constant d experiences a total increase of about 0.6 nm. The scattering intensity profile at 150 MPa is characteristic of F-actin. Upon further compression, the overall intensity of the scattering curve decreases, thus indicating formation of smaller filamentous species. An increase in temperature to 30 °C (see Figure S3) leads to a drastic decrease in pressure stability of the fascin-induced bundles. In this case, the peaks characteristic for bundles can be monitored up to a pressure of 125–160 MPa, only. However, for the Mg^{2+}-induced bundles, the effect of temperature on the pressure stability is much weaker. The observed denaturation pressure is around 160 MPa for all temperatures between 20 and 45 °C (see Figure S3B and C and Figure S5).

The apparent divergence of the d values upon approaching a critical pressure value (Figure 3 C and D) is reminiscent of the unbinding transitions observed in other soft elastic manifolds, including stacks of lipid bilayer membranes.[11] Such transitions arise from the competition of attractive molecular interactions and an effective interfilament repulsion which reflects the loss of configurational entropy within the bound state of the filaments. Lipowski and Leibler demonstrated that there exists a certain threshold below which the entropically driven undulations dominate the attractive forces, thus leading to complete unbinding.[11c] The apparent divergence of the d value approaching a critical pressure value in our case suggests a similar scenario, that is, $\langle d \rangle \propto (p_c - p)^{-\alpha}$ with an exponent α. The interplay of steric/electrostatic repulsion and attraction induced by fascin or Mg^{2+} determines whether the filaments bind or unbind. Changes in the intermolecular interaction are here because of the pressure-induced destabilization of the bridging fascin molecules and weakening of the electrostatic interactions in case of the Mg^{2+}-induced bundles. Assuming the validity of such scaling behavior leads to a critical exponent, α, of about 0.06 and to critical unbinding pressures, p_c, of about 310 and 160 MPa for the fascin- and Mg^{2+}-induced actin bundles, respectively. These values are in agreement with our experimental data. Interestingly, such unbinding scenario has also been observed in theoretical studies of bundles of semiflexible polymers such as actin filaments. Kierfeld et al. showed that the formation of bundles of parallel filaments requires a threshold concentration of linkers and the unbinding of bundles happens in a single, discontinuous transition.[12] In our case, the critical concentration of active linker molecules is modulated by pressure, and the critical behavior is in agreement with theoretical predictions.[12]

TEM measurements show that hydrostatic compression from 0.1 up to about 150 MPa does not significantly affect the morphology of both bundle types (Figure 4 A–D). Only a slight thinning and extension of the fascin-formed bundles can be observed (Figure 4 C). Interestingly, although highly ordered Mg^{2+}-induced bundles can be only found in situ up to a pressure of about 125 MPa, TEM reveals no morphological changes up to 150 MPa, thus indicating reversible pressure dissociation and therefore reassembly upon pressure release (Figure 4 D). Such a finding can be explained by the pressure effect on electrostatic interactions. Since dissociation of internal salt bridges leads to a reduction in the overall volume caused by electrostrictive effects of water molecules (due to formation of a dense hydration shell around the solvent-exposed ions),[13] attenuation of such interactions and thus an increase of the interfilament distance as observed in SAXS occurs upon pressure increase. Further pressure increase leads to complete and irreversible lateral dissociation of fascin-induced bundles into F-actin and finally formation of denatured protein clusters after pressure release (Figure 4 E and G). Similar to the temperature-dependent

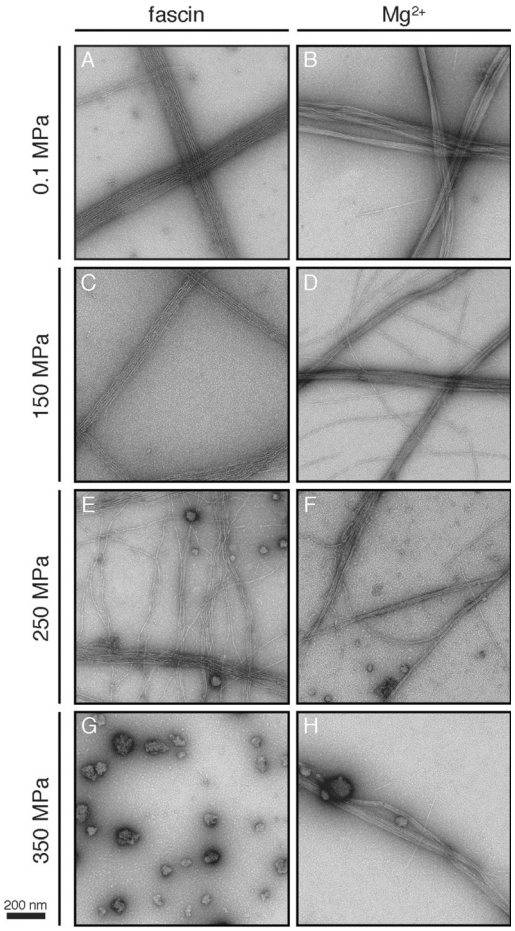

Figure 4. Pressure stability of fascin- and Mg^{2+}-induced B-actin. Representative transmission electron micrographs show the morphology of B-actin at ambient conditions (A and B) and after hydrostatic compression up to 150 (C and D), 250 (E and F), and 350 MPa (G and H) for 10 min.

behavior, F-actin is always present in the Mg^{2+}-induced assemblies and its concentration does not change below the denaturation pressure. Instead, a direct transformation from bundles to smaller protein clusters is observed ex situ (Figure 4F and H). These results indicate that hydrostatic compression causes denaturation of actin monomers directly within the bundles or after dissociation from the bundles. However, in comparison to the fascin-induced species, some Mg^{2+}-formed bundles can still be observed after pressurization up to 350 MPa (Figure 4G and H). Complementary low speed (20000 *g*) sedimentation assays reveal that thermal denaturation of both bundles leads to a continuous growth of the pellet fraction, thus indicating direct aggregation upon denaturation (see Figure S4). In contrast, pressure denaturation causes initial reduction of the pellet fraction and an increase again at higher pressure values, thus suggesting dissociation of intermediate species from the bundles which only aggregate above certain pressure values and after pressure release.

In conclusion, we have shown that bundles of long, parallel filaments that adhere through molecular cross-linkers like fascin or Mg^{2+} display different temperature and pressure stabilities owing to the different intermolecular interaction forces stabilizing the bundle structures. Both, the fascin-actin interaction and counterion organization, are not very sensitive to thermal fluctuations below T_M. The slight decrease of the *d* values, that is, lateral shrinkage of the bundles, might be due to minor protein conformational changes and/or changes in the level of hydration in the interfacial region. However, high hydrostatic pressure is known to lead to a weakening of electrostatic interactions.[13] As for Mg^{2+}-induced bundles electrostatic interactions are involved in the lateral condensation of F-actin, a pressure-induced weakening is expected to lead to the dissociation of the bundle structure. As a result of the closest packing of the filaments in the Mg^{2+}-bundles and small pressure-induced volume change upon disintegration,[10] packing defects are likely to be a minor factor. In contrast, the interfilament distance of the fascin-induced bundles is not affected upon pressurization up to about 100 MPa, and dissociation of the bundles sets in above approximately 250 MPa, only. This behavior indicates that additional interaction types are operative. As the stability of F-actin has been shown to be in the pressure range of 350 MPa,[10] destabilization of the tertiary structure of fascin and its local interaction site with F-actin is likely to be responsible for the dissociation of the fascin-stabilized bundles, which occurs at a pressure of about 250 MPa. Thus, compared to the divalent stabilized bundles, fascin-induced bundles feature a drastically higher pressure stability. Since both proteins, actin and fascin, are evolutionary highly conserved,[14] bundles formed by them might fit better the requirements inside cells for organisms living under extreme environmental conditions, such as those encountered in the deep sea, where pressures up to 110 MPa are reached.[15] Under such pressure conditions, the evolutionarily evolved actin-binding proteins, such as fascin, are required to ensure sufficient stability and mechanical resistance of the cytoskeleton.

Acknowledgements

The pressure-dependent SAXS experiments were performed on the ID02 beamline at the European Synchrotron Radiation Facility (ESRF), Grenoble, France. We are grateful to Dr. Johannes Möller at the ESRF for providing assistance in using beamline ID02. Financial support from the DFG Research Unit FOR 1979, and in part by the Cluster of Excellence RESOLV (EXC 1069) and the Fonds der Chemischen Industrie is gratefully acknowledged.

Keywords: biophysics · electron microscopy · high-pressure chemistry · polymers · proteins

How to cite: *Angew. Chem. Int. Ed.* **2015**, *54*, 11088–11092
Angew. Chem. **2015**, *127*, 11240–11244

[1] a) V. B. Teif, K. Bohinc, *Prog. Biophys. Mol. Biol.* **2011**, *105*, 208–222; b) C. E. Walczak, S. L. Shaw, *Cell* **2010**, *142*, 364–367; c) S. Khurana, S. P. George, *Cell Adhes. Migr.* **2011**, *5*, 409–420.
[2] a) V. A. Bloomfield, *Biopolymers* **1991**, *31*, 1471–1481; b) T. E. Angelini, H. Liang, W. Wriggers, G. C. L. Wong, *Proc. Natl. Acad. Sci. USA* **2003**, *100*, 8634–8637; c) J. X. Tang, P. A.

Janmey, A. Lyubartsev, L. Nordenskiöld, *Biophys. J.* **2002**, *83*, 566 – 581.
[3] L. Blanchoin, R. Boujemaa-Paterski, C. Sykes, J. Plastino, *Physiol. Rev.* **2014**, *94*, 235 – 263.
[4] a) M. M. A. E. Claessens, M. Bathe, E. Frey, A. R. Bausch, *Nat. Mater.* **2006**, *5*, 748 – 753; b) P. K. Mattila, P. Lappalainen, *Nat. Rev. Mol. Cell Biol.* **2008**, *9*, 446 – 454.
[5] T. E. Angelini, H. Liang, W. Wriggers, G. C. L. Wong, *Eur. Phys. J. E* **2005**, *16*, 389 – 400.
[6] a) S. B. Zimmerman, S. O. Trach, *J. Mol. Biol.* **1991**, *222*, 599 – 620; b) H.-X. Zhou, G. Rivas, A. P. Minton, *Annu. Rev. Biophys.* **2008**, *37*, 375 – 397.
[7] a) M. Hosek, J. X. Tang, *Phys. Rev. E* **2004**, *69*, 051907; b) R. Tharmann, M. M. A. E. Claessens, A. R. Bausch, *Biophys. J.* **2006**, *90*, 2622 – 2627.
[8] a) S. Jansen, A. Collins, C. Yang, G. Rebowski, T. Svitkina, R. Dominguez, *J. Biol. Chem.* **2011**, *286*, 300873 – 300896; b) S. Yang, F. K. Huang, J. Huang, S. Chen, J. Jakoncic, A. Leo-Macias, R. Diaz-Avalos, L. Chen, J. J. Zhang, X. Y. Huang, *J. Biol. Chem.* **2013**, *288*, 274 – 284; c) N. Kureishy, V. Sapountzi, S. Prag, N. Anilkumar, J. C. Adams, *BioEssays* **2002**, *24*, 350 – 361.
[9] a) M. M. A. E. Claessens, C. Semmrich, L. Ramos, A. R. Bausch, *Proc. Natl. Acad. Sci. USA* **2008**, *105*, 8819 – 8822; b) K. R. Purdy, J. R. Bartles, G. C. L. Wong, *Phys. Rev. Lett.* **2007**, *98*, 058105.
[10] C. Rosin, M. Erlkamp, J. von der Ecken, S. Raunser, R. Winter, *Biophys. J.* **2014**, *107*, 2982 – 2992.
[11] a) M. Benhamou, R. El Kinani, H. Kaidi, *Conf. Pap. Eng.* **2013**, *2013*, 320718; b) M. Benhamou, H. Kaidi, *Eur. Phys. J. E* **2013**, *36*, 125; c) R. Lipowsky, S. Leibler, *Phys. Rev. Lett.* **1986**, *56*, 2541 – 2544.
[12] a) J. Kierfeld, T. Kühne, R. Lipowsky, *Phys. Rev. Lett.* **2005**, *95*, 038102; b) J. Kierfeld, R. Lipowsky, *J. Phys. A* **2005**, *38*, L155 – L161.
[13] a) J. L. Silva, D. Foguel, C. A. Royer, *Trends Biochem. Sci.* **2001**, *26*, 612 – 618; b) R. Mishra, R. Winter, *Angew. Chem. Int. Ed.* **2008**, *47*, 6518 – 6521; *Angew. Chem.* **2008**, *120*, 6618 – 6621; c) K. Akasaka, *Chem. Rev.* **2006**, *106*, 1814 – 1835.
[14] a) P. W. Gunning, U. Ghoshdastider, S. Whitaker, D. Popp, R. C. Robinson, *J. Cell Sci.* **2015**, *128*, 2009 – 2019; b) R. S. Sedeh, A. A. Fedorov, E. V. Fedorov, S. Ono, F. Matsumura, S. C. Almo, M. Bathe, *J. Mol. Biol.* **2010**, *400*, 589 – 604.
[15] a) I. Daniel, P. Oger, R. Winter, *Chem. Soc. Rev.* **2006**, *35*, 858 – 875; b) F. Meersman, I. Daniel, D. H. Bartlett, R. Winter, R. Hazael, P. F. McMillan, *Rev. Mineral. Geochem.* **2013**, *75*, 607 – 648.

Received: May 9, 2015
Revised: June 11, 2015
Published online: August 5, 2015

